Deep-Sea Research Part II 144 (2017) 6–20

Contents lists available at ScienceDirect

Deep-Sea Research Part II

journal homepage: www.elsevier.com/locate/dsr2

The summer hydrographic structure of the Hanna Shoal region on the northeastern Chukchi Sea shelf: 2011–2013

Thomas Weingartner[a,*], Ying-Chih Fang[a], Peter Winsor[a], Elizabeth Dobbins[a], Rachel Potter[a], Hank Statscewich[a], Todd Mudge[b], Brita Irving[a], Leandra Sousa[c], Keath Borg[b]

[a] College of Fisheries and Ocean Sciences, University of Alaska, Fairbanks, AK 99775, USA
[b] ASL Environmental Sciences, Inc., #1-6703 Rajpur Place, Victoria, B.C., Canada V8M 1Z5
[c] North Slope Borough, Department of Wildlife Management, P.O. Box 69, Barrow/Utqiaġvik, AK 99723 USA

ABSTRACT

We used shipboard and towed CTD, current meter, and satellite-tracked drifter data to examine the hydrographic structure in the northeastern Chukchi Sea in August–September of 2011, 2012, and 2013. In all years the densest winter water was around and east of Hanna Shoal. In 2012 and 2013, a ~ 15 m deep layer of cold, dilute meltwater overlaid the dense water north of the shelf region between ~ 71.2 and ~ 71.5°N. A front extends from the southwest side of Hanna Shoal toward the head of Barrow Canyon, separated meltwaters from warmer, saltier Bering Sea Summer Waters to the south. Stratification was stronger and the surface density variances in the meso- and sub-mesoscale range were higher north of the front than to the south. No meltwater or surface fronts were present in 2011 due to a very early ice retreat. Differences in summer ice cover may be due to differences in the amount of grounded ice atop Hanna Shoal associated with the previous winter's regional ice drift.

Along the north side of Hanna Shoal the model-predicted clockwise barotropic flow carrying waters from the western side of the Shoal appears to converge with a counterclockwise, baroclinic flow on the northeast side. The baroclinic tendency is confined to the upper 30 m and can include waters transported from the shelfbreak. The inferred zonal convergence implies that north of the Shoal: a) near-surface waters are a mixture of waters from the western and eastern Chukchi Sea and b) the cross-isobath pressure gradient collapses thereby facilitating leakage of upper layer waters northward across the shelf.

1. Introduction

Pacific waters flowing northward through Bering Strait and across the Chukchi Sea spread poleward across three principal bathymetric depressions: Herald Valley in the west, the Central Channel in mid-shelf, and Barrow Canyon along the Alaskan coast (Fig. 1a). Hanna Shoal lies between the latter two features (Fig. 1b). Its western side abuts the northern end of the Central Channel, while its eastern flank yields to an 80 km wide bench along the western wall of Barrow Canyon. The Shoal is a west-east oriented oval ~ 150 km long and ~ 55 km wide (based on the 40 m isobath). The shelfbreak (~ 100 m isobath) lies 75 km to the north, and the broad, gently sloping central shelf of 40–45 m depth is to the south. Minimum depths atop the Shoal are ~ 20 m and shallow enough to ground sea ice with deep keels, as evidenced by the heavily scoured gravelly seabed (Grantz and Eittreim, 1979).

Circulation models (Winsor and Chapman, 2004; Spall, 2007) depict the average flow as northward in the Central Channel and Herald Valley (Fig. 1a), with the outflows from both proceeding eastward over the outer shelf and shelfbreak. Some of this eastward flow is predicted to continue clockwise around the southeast side of Hanna Shoal before retroflecting eastward. Upon retroflecting, this flow merges at the head of Barrow Canyon with eastward flow over the central shelf and northeastward flow along the coast (Fig. 1a; Weingartner et al., 2017; Fang et al., 2017). The models suggest that southward flow on the east side and over Hanna Shoal is weaker than the flow along its northern and southern flanks, which is consistent with the spreading of the isobaths between the western and eastern sides of the Shoal. Martin and Drucker (1997) attributed the weak flow over the Shoal to Taylor column formation and suggested that this feature was one reason why ice persists here well after it has retreated elsewhere on the shelf. The summertime persistence of sea ice over Hanna Shoal is of considerable ecological importance as the area supports a large number of ice-obligate and ice-associated species (Moore and Huntington, 2008; Moore

* Corresponding author.
E-mail address: tjweingartner@alaska.edu (T. Weingartner).

http://dx.doi.org/10.1016/j.dsr2.2017.08.006

Available online 17 August 2017

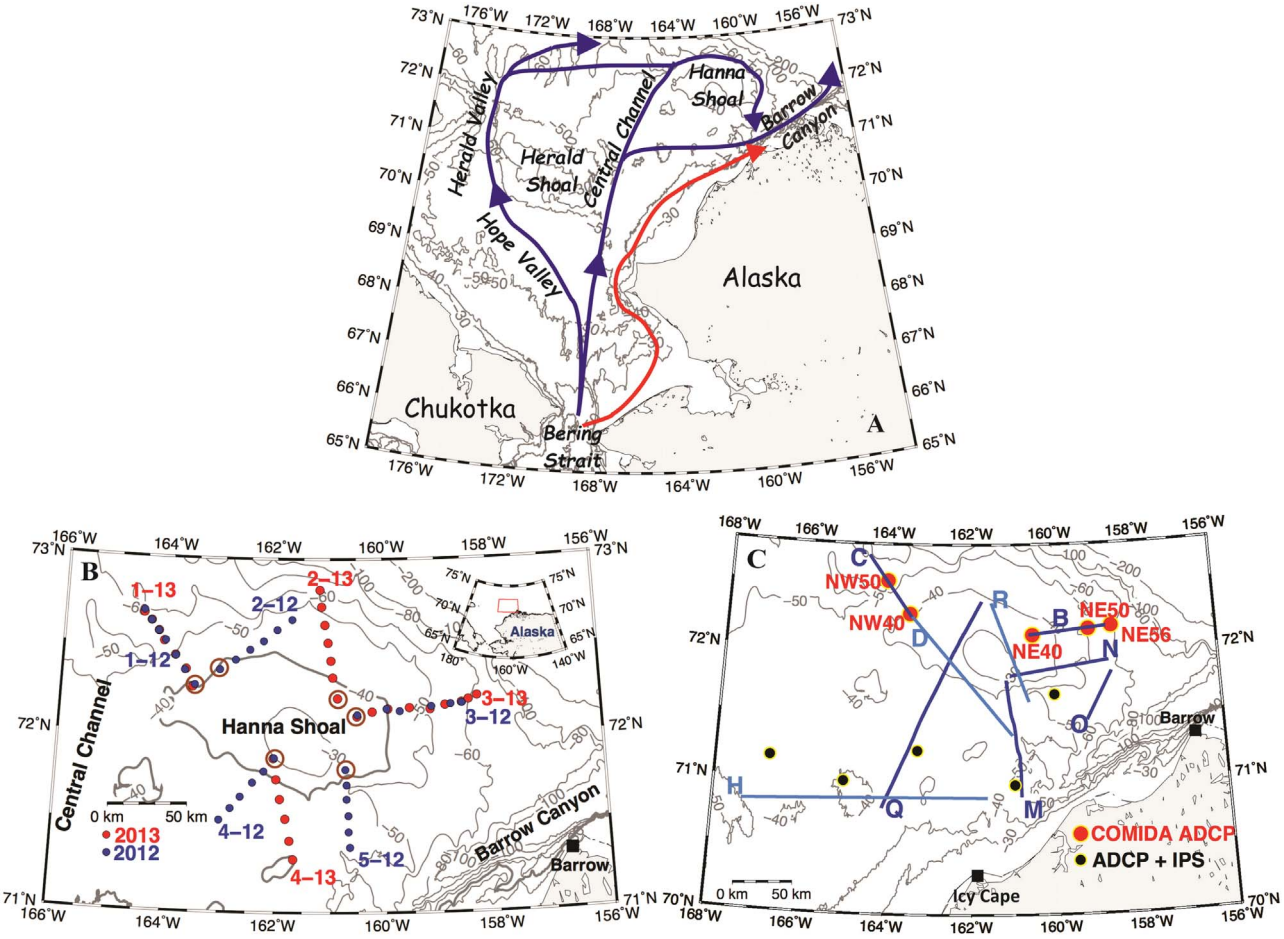

Fig. 1. A) Bathymetric map of the Chukchi Sea showing principal flow pathways northward from Bering Strait. The pathway denoted by the red arrow denotes the Alaskan Coastal Current, which carries the freshest and warmest fraction of the Bering Strait outflow and the blue arrows denote the pathways for the cooler and saltier fractions. B) Map of Hanna Shoal and the surrounding shelf showing locations of 2012 (blue) and 2013 (red) CTD stations. C) Location of various current meter and ice profiling sonar (IPS) moorings (symbols) and Acrobat towed-CTD transects (blue lines). (For interpretation of the references to color in this figure legend, the reader is referred to the web version of this article.)

et al., in press). These species are sustained by the high benthic biomass found throughout the region, with particularly large numbers of benthic organisms found on the southeast side of the Shoal (Blanchard et al., 2013; Schonberg et al.,2014).

This study was motivated by the need to provide observations for evaluating ocean circulation models in a region of the Chukchi shelf susceptible to potential impacts from offshore oil development. Moreover, Pacific-derived waters undergo substantial modification while crossing this shelf and not all the flow pathways and modification sites are understood. In particular, the region around Hanna Shoal has received limited attention because heavy ice has often impeded sampling here. We describe interannual variations in the regional hydrographic structure of the northeastern shelf in summer (August–September) and examine the connectivity in the circulation between the west and east sides of the Shoal. Section 2 outlines the data sets used, which span the years from 2011 to 2013. In Section 3.1, we summarize the summer wind and ice conditions in these years. We next provide an overview of the hydrography of the central shelf and Hanna Shoal region with an emphasis on differences between summers with light and heavy ice concentration (Section 3.2). Section 3.3 examines in greater detail the differences in hydrographic and circulation structure between the western and eastern sides of the Shoal. Section 4 discusses the results and suggests reasons for the marked differences in summer ice concentrations between 2011 and the later years.

2. Data and methods

2.1. Hydrography

Three different hydrographic data sets, each averaged into 1-db vertical bins, are used. The first consists of shipboard CTDs collected during the Chukchi Offshore Monitoring in Drilling Area (COMIDA) program from the USCGC *Healy* in 2012 and 2013 (Fig. 1b). The station spacing varied but was typically ~ 10 km. Time constraints prevented us from conducting extensive CTD surveys south of Hanna Shoal during both COMIDA cruises. To place the COMIDA CTD data in a broader spatial and temporal context, we use CTD data collected on separate cruises under the auspices of the Chukchi Sea Environmental Studies Program (CSESP; sponsored by the oil industry) in August and September of 2011, 2012, and 2013. The August cruises were confined to small study areas over the shelf south of Hanna Shoal, whereas the September cruises enabled broader surveys that extended to the north and east of Hanna Shoal. CTD processing followed the procedures of Weingartner et al. (2013). The August and September cruises occurred at identical times in each year, with the sampling progressing from south to north across the domain. Although not synoptic, the data underscore the large interannual differences in the seasonal hydrography of this region. The third data set consists of several high-resolution (~ 250 m) Acrobat towed CTD and fluorometric sections (Fig. 1c) supported by the Bureau of Ocean Energy Management (BOEM) and processed per Martini et al. (2016). The sensors were calibrated at the factory prior to the cruise and the chlorophyll values are estimated

based on this calibration because no chlorophyll samples were collected on these cruises. The chlorophyll *a* concentrations are to be regarded as relative, not absolute, values.

2.2. Meteorology, sea ice concentrations, drift, and thickness and satellite-tracked drifters

We used winds and sea level pressures forecast at 3-h intervals from NOAA's North American Regional Reanalysis (NARR) models (Mesinger et al., 2006). Sea ice concentration maps for June and July, from 2011 to 2013, were constructed from data obtained by the Advanced Microwave Scanning Radiometer (AMSR-E), Special Sensor Microwave Imager (SSMI) satellite sensor, and the Advanced Microwave Scanning Radiometer-2 (AMSR2), respectively and processed according to Spreen et al. (2008). More detailed maps of the ice edge for the August – September periods of each year were prepared based on National Ice Center (NIC) analyses. Through CSESP, the oil industry supported paired ice-profiling sonar (IPS) and ADCP moorings to measure ice thickness and drift respectively during the winters of 2011–13 at several locations south of Hanna Shoals (Fig. 1c). The IPS processing follows Melling et al. (1995) and a detailed description of the processing procedures for the IPS and ADCP data is given by Mudge et al. (2015). In Section 4 we use the mean ice keel values computed over the upper 25% of the keel depth frequency distribution. Following Melling et al. (1995), the latter were formed from 50 km-long sections based on the ice drift. We then computed monthly means based on these values assigning segments that spanned across months to the month in which the majority of the segment occurred. The COMIDA program also included current data from five moored ADCPs positioned on the northwest and northeast sides of Hanna Shoals, 2012–14 (Fig. 1c). We use subsets of these data coincident in time with the COMIDA CTD sections. A more in-depth analysis of these and the CSESP moorings will be the focus of a future paper.

In addition, we show trajectories from a subset of 13 satellite-tracked Microstar drifters (manufactured by Pacific Gyre, San Diego CA) equipped with a CODE-type drogue (Davis, 1985) at 1-m depth. The drifters were deployed concurrently near Icy Cape (Fig. 1c) and within ~ 15 km of the Alaskan coast on 12 August 2012. Processing details and additional descriptions are given by Weingartner et al. (2015).

3. Results

3.1. Sea ice conditions

Fig. 2 shows maps of the shelf-wide distribution of sea-ice

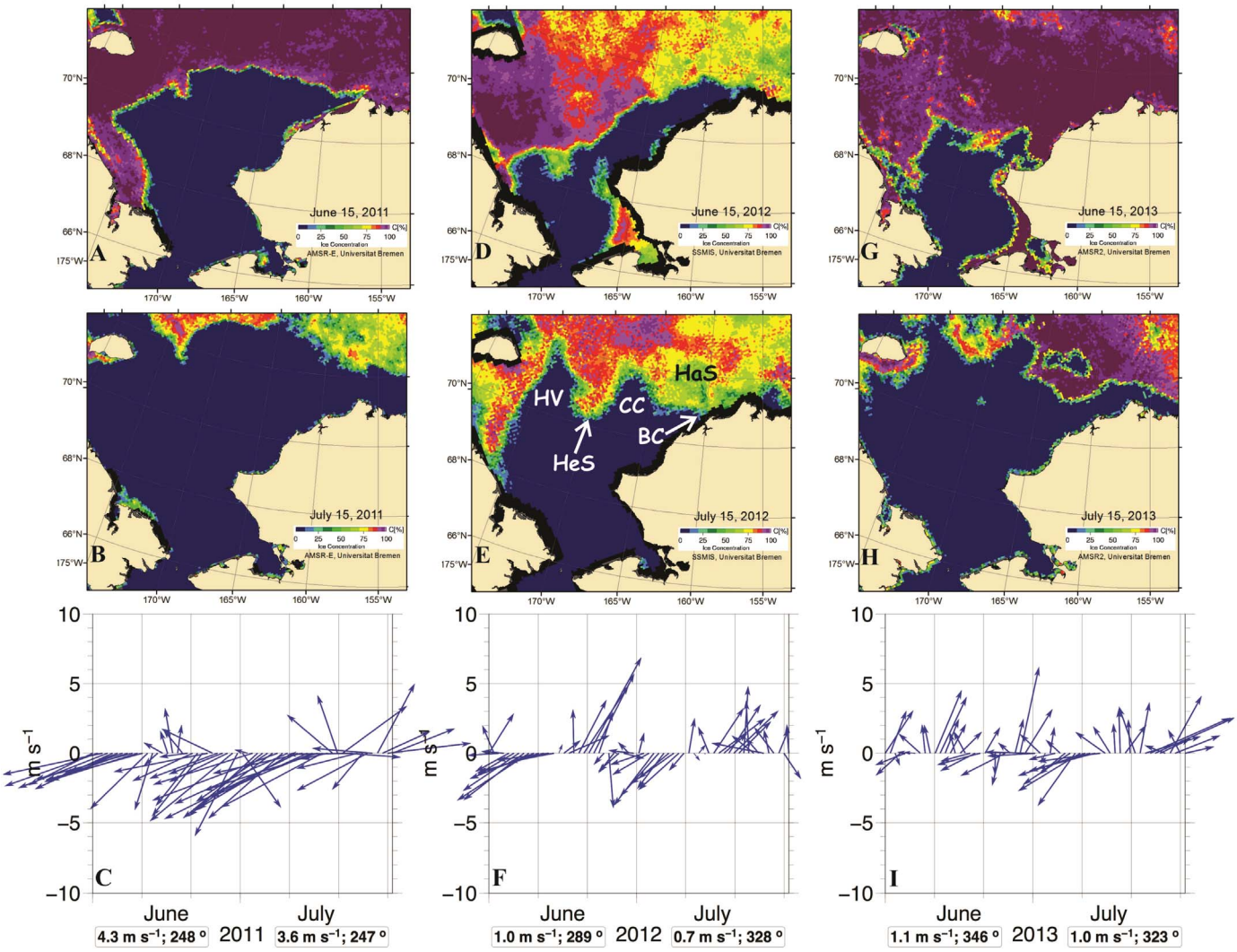

Fig. 2. Sea ice concentration maps on 15 June (top) 15 July (middle) and mean daily wind vectors (bottom). Panels a, b and c are for 2011, d, e, and f are for 2012, and g, h, and i are for 2013. The features labelled in map E are: Herald Valley (HV), Herald Shoal (HeS), Central Channel (CC), Hanna Shoal (HaS), and Barrow Canyon (BC). Wind vector plots include mean monthly wind velocity and wind speed in parentheses.

concentrations in mid-June and mid-July of 2011–2013 and time series of the mean daily winds for June and July. In 2011, the ice retreat occurred early insofar as the Chukchi shelf south of 71°N was largely ice-free by mid-June (Fig. 2a). The remainder of the Chukchi shelf and the western Beaufort Sea were ice free by mid-July (Fig. 2b). Northeasterly winds prevailed in both months (Fig. 2c). In 2012, winds varied from northeasterly to southwesterly but were from the southeast on average (Fig. 2f). By mid-June 2012, the western Chukchi had heavy ice concentrations, but a broad swath of the northeast shelf was ice-free (Fig. 2d). By mid-July, the ice had retreated northward over the western shelf but advanced southward over portions of the northeast shelf (Fig. 2e). In addition, distinct embayments formed in Herald Valley, the Central Channel, and Barrow Canyon with the ice edge oriented from west to east between the Channel and the Canyon along ~ 71°N. The embayments, discussed by Paquette and Bourke (1981) and Martin and Drucker (1997), correspond to the principal flow pathways along which warm Bering Sea Summer Waters (BSSW) cross the shelf. These indentations are annually recurring features and were well-known to 19th century whalers (Bockstoce, 1986). They vary in extent from year-to-year and are separated from one another by heavier ice concentrations over Herald and Hanna shoals (Fig. 2e). In mid-June 2013 (Fig. 2g), the ice-edge had retreated to ~ 70°N over the central shelf, but heavy concentrations remained elsewhere.

By mid-July 2013 (Fig. 2h, the western Chukchi was largely ice-free with open water present at the northern end of the Central Channel (along 73°N, between 165° and 170°W) and over Barrow Canyon, although heavy ice concentrations remained over Hanna Shoal. In both months winds were variable but primarily southerly (Fig. 2i).

The subsequent evolution of ice concentrations in the Hanna Shoal region is given by biweekly maps of the 15% ice concentration isopleth (as estimated by NIC) for the August-September period of each year along with the corresponding mean daily NARR winds for the same period (Fig. 3). In 2011, the region was virtually ice-free and remained so through September. In 2012, ice remained over Hanna Shoal through mid-September. The same basic pattern persisted in 2013, although the ice rapidly retreated from south of Hanna Shoal on 1 September to the northwest of the Shoal by mid-September. The ice conditions of Fig. 3 were not obviously related to the concurrent winds. For example, in both 2011 (ice-free year) and 2013 (moderate to heavy ice year) the winds were persistently from the northeast and moderately strong (~ 5 to 10 m s^{-1}).

In contrast, in 2012 (heavy ice year) the winds were from the south through August and then northeasterly through most of September. During the 2012 and 2013, COMIDA cruises observations from the *Healy* bridge suggested extensive grounding of very thick ice atop Hanna Shoal, which limited sampling here. Possible causes for these interannual variations in the Hanna Shoal ice cover will be considered in Section 4.

3.2. Hydrography: broad-scale perspective

We begin by examining plan views of the vertically-averaged upper and bottom 10 m of the water column in both August and September 2012 (Fig. 4) because we believe that these conditions are typical of the Hanna Shoal region (Weingartner et al., 2013). There are several water mass classifications for the Chukchi Sea shelf (e.g., Coachman, Aagaard, and Tripp, 1975; Gong and Pickart, 2014). For our purposes we define BSSW as consisting of a warm (> 4 °C) and dilute (~ 31 to 32) fraction and a colder (2–4 °C) and saltier (32–32.5) fraction. The warmer waters are typically carried northward in the Alaskan Coastal Current (red arrow in Fig. 1a), while the cooler and saltier fraction is transported through the Central Channel and Herald Valley. In addition, the shelf contains ice meltwaters (MW), which are cold (< 2 °C) and fresh (24 to ~ 30) and winter waters (WW), which are < −1.0 °C and salty (> 32.5). WW is near-freezing when produced in winter on the Bering and Chukchi shelves as a result of ice formation and can warm slightly in summer months (Gong and Pickart, 2014). The disposition of these water masses varies seasonally. WW is pervasive in winter but is

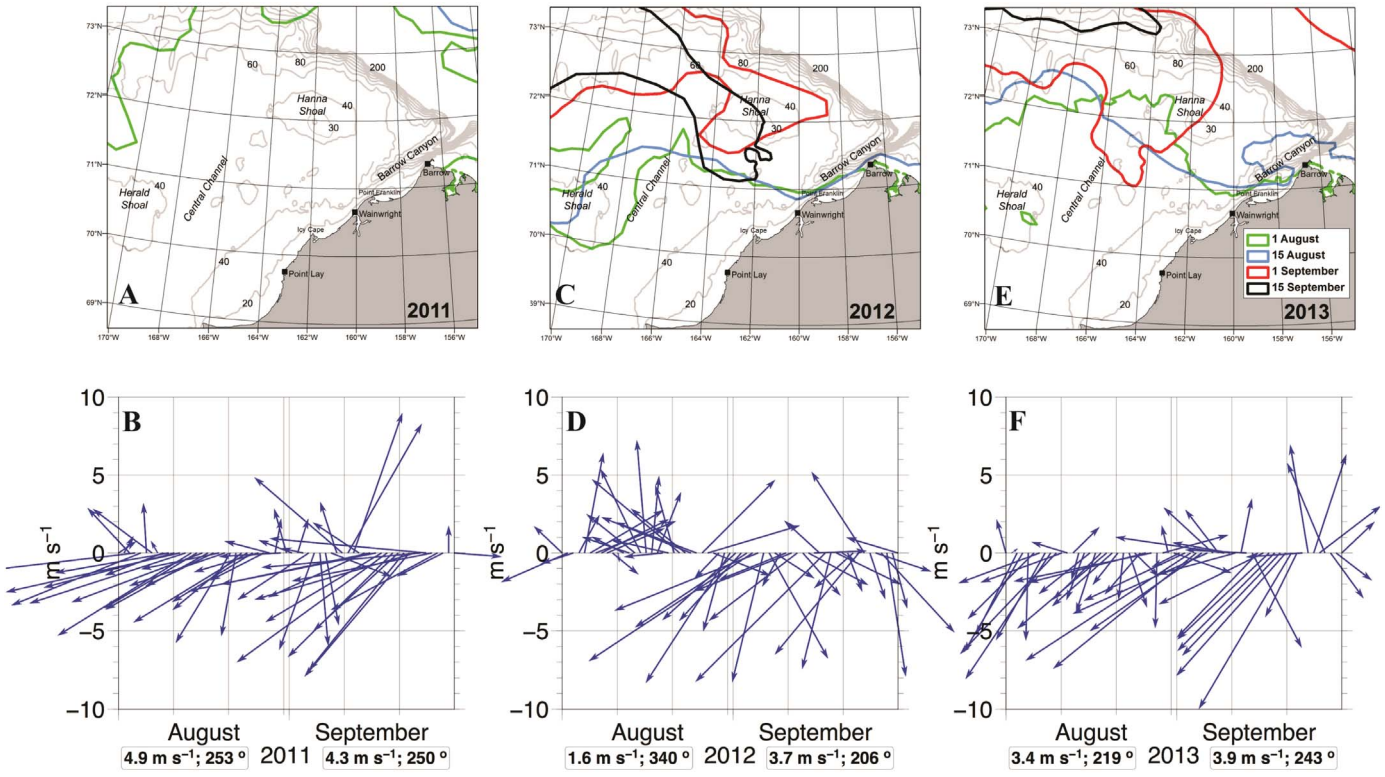

Fig. 3. Maps of the 15% ice concentration isopleth at biweekly intervals for the August–September period (top row) and mean daily wind vectors (bottom row). Panels a and b are for 2011, c and d are for 2012, and e and f are for 2013. The mean monthly wind velocity and wind speed (in parentheses) are listed below the x-axis for each year.

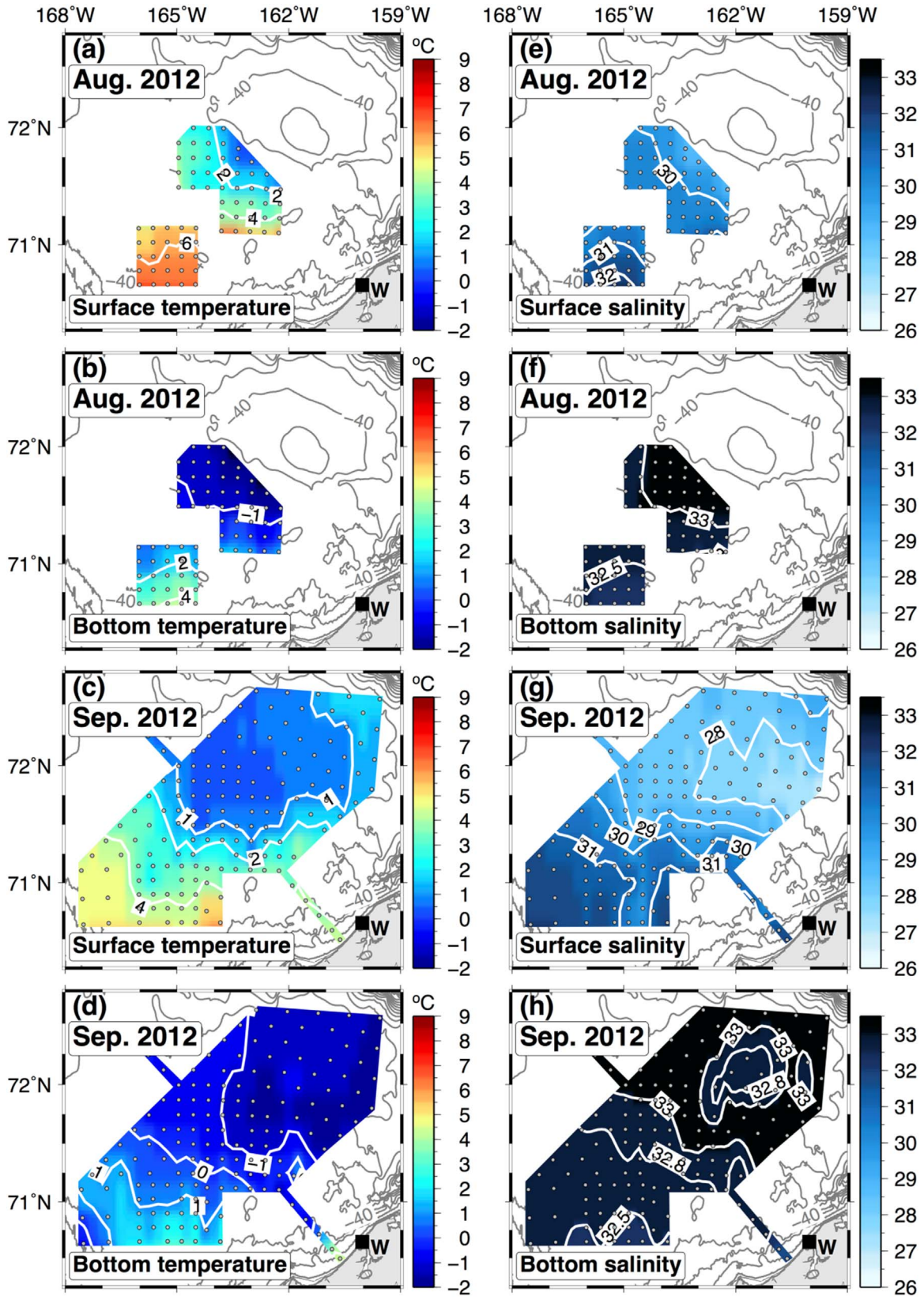

Fig. 4. Plan views of temperature (left) and salinity (right) in August and September of 2012 based on averages of the upper and bottom 10 m of the water column. The village of Wainwright is designated with a "W". Filled circles show CTD station locations.

gradually displaced northward with the springtime increase in transport through Bering Strait (Weingartner et al., 2005; Woodgate et al., 2005) and by late summer occurs over the northern half of the shelf underlying MW and/or BSSW (Weingartner et al., 2013; Pickart et al., 2016).

In August, the surface waters from ~ 70.5° to 71°N and between

164° and 165°W were warm (~ 6 °C) and moderately salty (31–32). Bottom waters were slightly colder with both water masses consistent with BSSW advected northward from Bering Strait in summer. North of this location and south of Hanna Shoal, surface waters were cool (2–4 °C) and fresh (~ 30), suggestive of MW, perhaps warmed by solar radiation and/or mixed with BSSW. North of ~ 71.25°N bottom waters were the very cold (< − 1 °C) and salty (> 32.8) WW. The more complete coverage of September 2012 illustrates the enormous spatial extent of the surface MW, which occupied the entire region north of ~ 71.5°N. South of this latitude, the shelf contained BSSW, with this water mass extending northward in the Central Channel along 166°W as well as eastward toward the coast near Wainwright. Overall these data suggest a front which extends southward from 72°N, 166°W (approximately parallel to the Central Channel) and then trending eastward along 71.5°N towards Barrow Canyon. Very likely this meltwater front is part of the same frontal system that extends along the length of Barrow Canyon (Pickart et al., 2005; Gong and Pickart, 2014). The spatial distribution of WW along the bottom in September was similar in extent to the surface MW, although WW extended farther inshore than MW. Note also that the coldest WW formed an arc along the southern and eastern sides of Hanna Shoal. The 2013 CSESP hydrography (Weingartner et al., 2014) was broadly similar to that of 2012 in terms of the areal distributions of the major water masses and location of the MW/BSSW frontal system along ~ 71.5°N. The major difference was that bottom salinities were slightly fresher (32.5–32.8) compared to 2012.

Water mass distributions in 2011 were quite different in several important respects (Fig. 5). Most obvious was the complete absence of MW, which is not surprising given the early retreat of sea ice in 2011 (Figs. 2 and 3). The surface layer in both August and September consisted entirely of BSSW, was nearly homogeneous in salinity, lacked surface fronts, and had only weak meridional thermal gradients. In August 2011, the bottom waters between 70–71°N and 164–165°W were BSSW, while WW occupied the shelf north of this location and along the southern side of Hanna Shoal. In September, BSSW was prominent at the surface and bottom in the Central Channel, over the shelf south of ~ 71°N, and was even found over the shallowest portions of Hanna Shoal, although the low salinities here could have been a remnant of MW that had either mixed with the BSSW or had warmed. Except as noted with respect to the Central Channel, WW surrounded most of Hanna Shoal. It extended as far south as 71°N with the coldest waters forming a prominent lobe on the southern side of Hanna Shoal. A thermohaline bottom front separated this WW from the adjacent BSSW. The WW properties in 2011 were fresher (~ 32.5) than the corresponding WW salinities > 32.8 of 2012 (Fig. 4h).

An alternative perspective of the contrasting thermohaline structure between these two years is given by Fig. 6, which consists of two, 300-km long vertical sections occupied in September 2011 and 2012. The transect (shown in Fig. 5c) extended from the southwest (~ 70.5°N, 166°W) to the northeast (~ 72.5°N, 160°W) with the northern portion of the transect along the eastern side of Hanna Shoal. In 2011, warm, moderately salty BSSW entirely encompassed the upper 20 m of the water column and along the bottom over the first 100 km. WW was present below ~ 20 m on the northern and southern sides of Hanna Shoal and was separated from BSSW in the south by a bottom temperature front. In contrast, the 2012 section consisted of a strong frontal system associated with MW and BSSW at 140 km, in addition to weaker MW fronts at 175 km and 200 km. The sections also differ with respect to the vertical stratification, which in both years was dominated by the vertical salinity gradient. The stratification in 2012 (and 2013) was nearly twice as strong as in 2011, with these differences primarily due to the absence of MW in 2011 and its presence in 2012 (and 2013).

Another notable feature in the 2012 section was the presence, at km 225, of a “lens” of warm (~ 2 °C) water, signified by an upward distension of the 29 isohaline above the lens and a less prominent, downward-bowing of the 32 isohaline below. This feature is likely an anticyclonic, intrapycnocline eddy formed via a baroclinic instability of the MW/BSSW front. These features are often observed when MW/BSSW fronts are present and are probably important agents for lateral mixing (Lu et al., 2015).

The coarse resolution of the CSESP CTD sampling did not permit adequate horizontal resolution of the MW/BSSW fronts but Acrobat sections collected in September 2013 along Legs Q and M (Fig. 1b) resolve the frontal width scale. In both cases, the front was ~ 10 km wide and located at ~ 71.5°N on Leg Q and 71.2°N on Leg M (Fig. 7a, b, c, and d). We examined the stability of these fronts using the balanced Richardson number criterion (Thomas et al., 2016) and found that portions of the MW/BSSW front (including some sections not presented here) met the necessary conditions for symmetric instability, whereas other segments did not. The results are equivocal and, at best, suggest that there was spatio-temporal variability along the front with respect to this criterion.

The chlorophyll distributions (Fig. 7e, f) along these sections are interesting in two regards. First, the densest chlorophyll concentrations occur in the highly-stratified region north of the front on the 26 σ_θ isopycnals at ~ 25 m depth, and below the pycnocline. Second, the chlorophyll distribution appears very patchy with the patch scales ranging from ~ 1 to ~ 20 km based upon visual inspection. Nutrient concentrations, reported by Codispoti et al. (2005), Questel et al. (2013), and Danielson et al. (2017) indicate that WW bottom waters have sufficiently high nutrient levels to sustain primary production, while MW is nutrient deficient. Although high in nutrients upon leaving Bering Strait, BSSW nutrient levels are depleted by the time these waters reach the northeastern Chukchi shelf in August and September. Consequently, neither the absence of chlorophyll in the surface waters or the sub-surface chlorophyll maxima in the heavily stratified MW/WW is surprising. There is, however, no indication of chlorophyll patchiness or of a well-defined sub-surface chlorophyll maximum in the less-stratified regions south of the front where BSSW overlies WW.

These (and other) Acrobat sections suggest that the surface layer containing BSSW south of the front is horizontally homogenous in contrast to the more heterogeneous surface layer north of the front. Indeed, Fig. 7 suggests that north of the main front, there were weaker and equally shallow fronts composed solely of meltwater of varying salinities and temperatures. We quantified these differences by computing the wavenumber spectra of density at 10 m depth (similar to Timmermans and Winsor, 2012). The spectra were computed north and south of the front from different acrobat sections (Fig. 1b) but not across the front. We then integrated the spectra over three different spatial bands (1–5 km, 5–10 km, and 10–20 km) and compared the variance in each band. Regionally the baroclinic radius of deformation is ~ 5 km, so we define the mesoscale portion of the spectrum as having length scales of > 5 km and the sub-mesoscale range having length scales < 5 km. The computations were done separately using sections north and south of the front and the results summarized in Fig. 8. South of the front, the variance was uniformly low across the entire spectral range, with typical values being 1–2 $kg^2\,m^{-6}$. North of the front, the variances increase, although not consistently across all the sections. In general, the variances north of the front were a factor of 2–5 times greater in these bands than the variances south of the front. Quite possibly this greater spatial variability includes vertical motions over similar spatial scales that contribute to the patchiness in the chlorophyll distributions.

3.3. Hydrography: Hanna Shoal

In this section we examine the temperature and salinity structure around the Shoal based on CTD sections occupied during the 2012 and 2013 mid-August COMIDA cruises. In both years heavy ice and other time constraints limited the spatial coverage. We occupied five sections in 2012 and four sections in 2013 (Fig. 1b), with each section radiating outward from the Shoal. The 2012 sections included three Sections

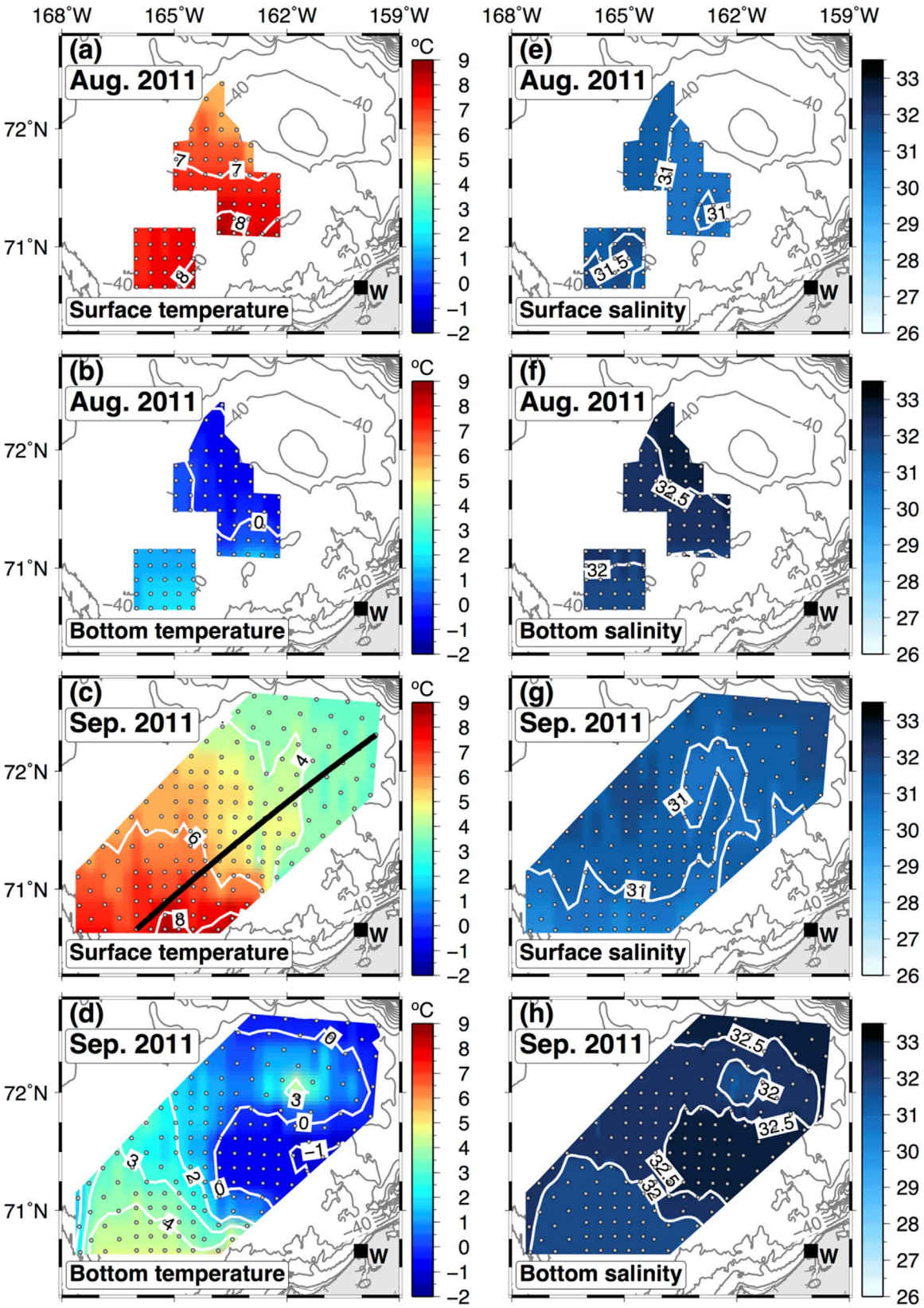

Fig. 5. Plan views of temperature (left) and salinity (right) from August and September 2011 based on averages of the upper and bottom 10 m of the water column. The village of Wainwright is designated with a "W". Filled circles show CTD station locations. The black line in panel c shows the location of the vertical sections from 2011 and 2102 shown in Fig. 6.

(1–12, 2–12, and 3–12) arrayed from west to east on the northern side of the Shoal (Fig. 9) where ice concentrations were 60 – 80%, except along the inner portion of Section 1–12 where concentrations were ~30%. Winds during the 2012 sampling were southerly at ~ 4 m s^{-1}. Under these conditions the flow over the shelf south of the front was likely eastward at 5–10 cm s^{-1}, veering northeastward and becoming

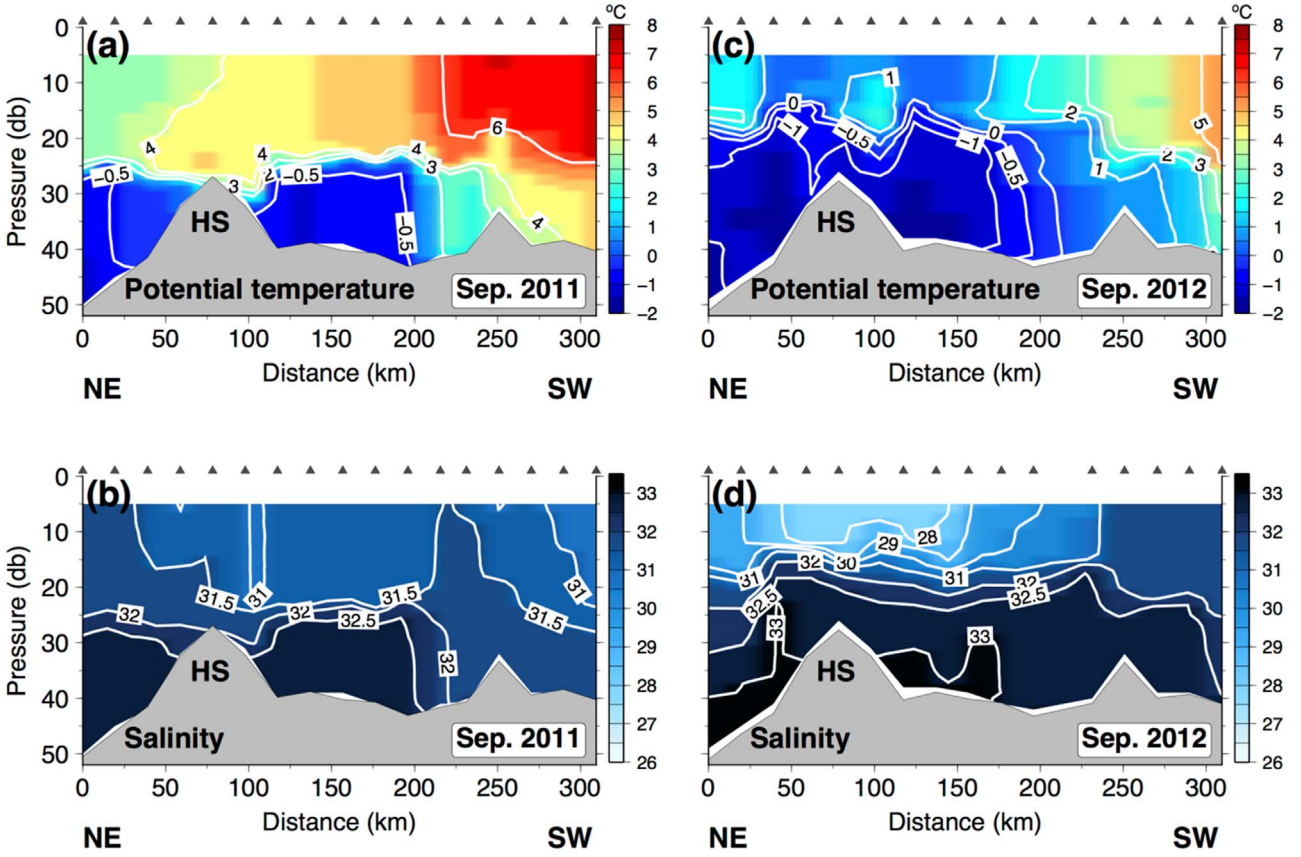

Fig. 6. Vertical sections of potential temperature (top row) and salinity (bottom row) collected from early to late of September 2011 (a, b) and 2012 (c, d), respectively. The location of both sections is shown in Fig. 5c. Hanna Shoal is denoted as "HS". Inverted triangles indicate station locations.

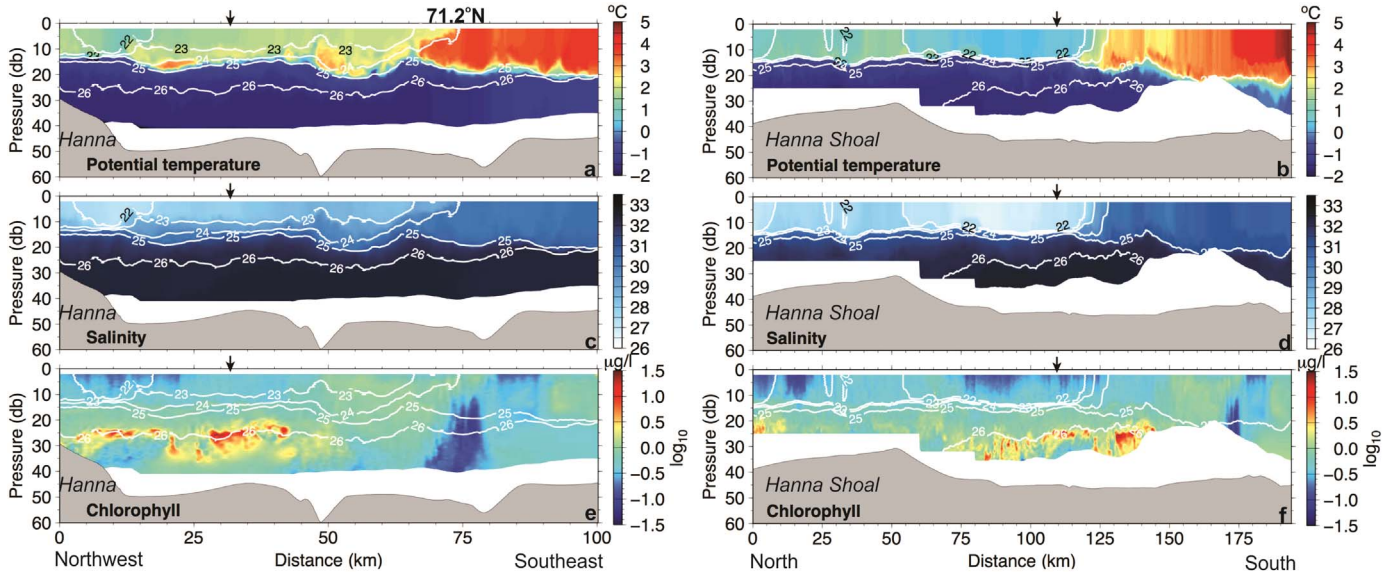

Fig. 7. Vertical sections of potential temperature (a, b), salinity (c, d), and fluorescence expressed as ug-l^{-1} of chlorophyll *a* (e, f) in September 2012 along Leg M (left) and Leg Q (right). The white contours indicate σ_θ isolines. The arrows at the top of each figure indicate latitude 71.5°N. The locations of these transects are shown in Fig. 1c. The front along Leg M is located at 71.2°N as indicated.

swifter along the coast (Weingartner et al., 2013) while the surface currents east of Hanna Shoal were weakly eastward at 2–5 cm s^{-1} (Weingartner et al., 2017; Fang et al., 2017). Similar sections were occupied in 2013 (Fig. 10, but note that Section 2–13 differs in location from Section 2–12, Fig. 1a). Winds during the 2013 sampling were northeasterly at ~ 4 m s^{-1}, in which currents should also be eastward south of the front at ~ 5 cm s^{-1} (Weingartner et al., 2013), but westward at ~ 5 cm s^{-1} at the surface east of Hanna Shoal (Fang et al., 2017). Thus we feel that in both years the sections were sampled synoptically during the occupation of the COMIDA transects. Ice concentrations along these sections were similar to those of 2012, except the concentrations were generally 0–30% along Section 1–13. Fig. 11 shows Sections (4–12, 5–12, and 4–13) on the southern side of the Shoal, where there was heavy ice along the northern part of each

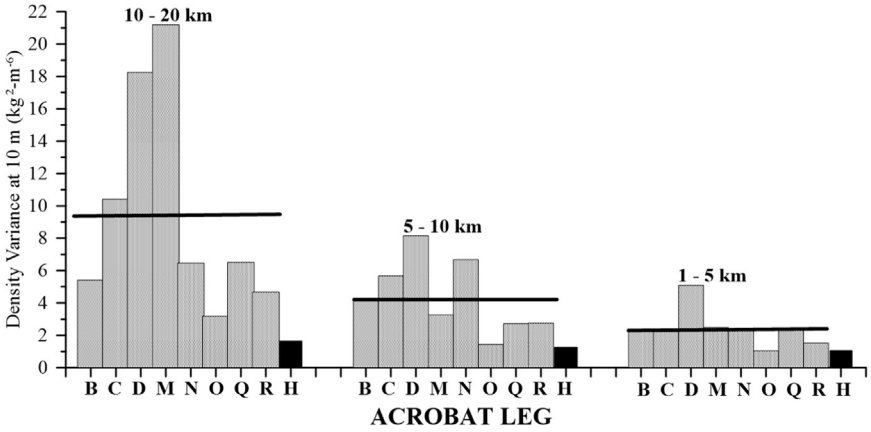

Fig. 8. Histograms of density variance at 10 m depth as a function of horizontal length scale based on 2013 Acrobat CTD tows collected north of the front (gray stippled bars) and south (black bars) of the front. The horizontal bars denote the mean density variance in each band for the gray bars.

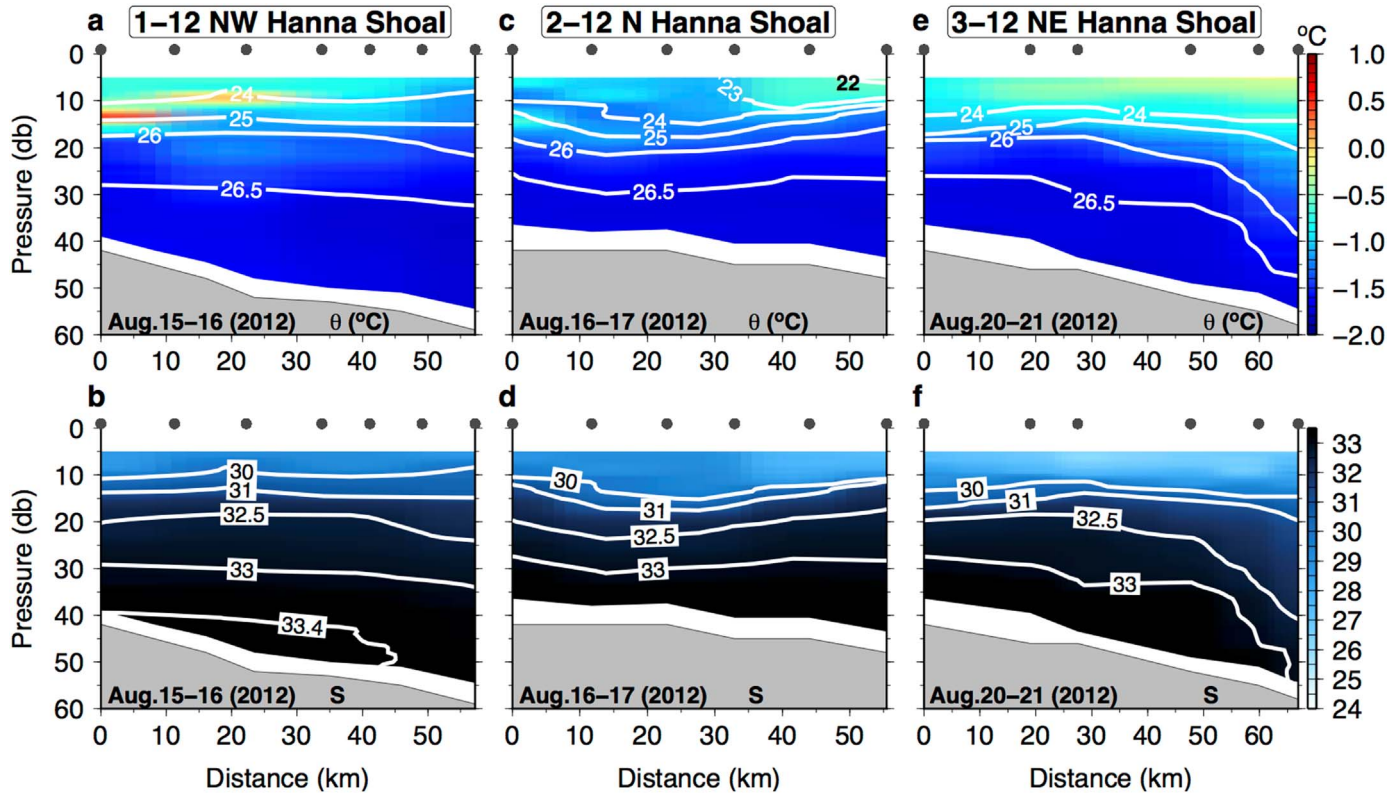

Fig. 9. Vertical sections of potential temperature (θ; top) and salinity (S; bottom) along transects 1–12 (a, b), 2–12 (c, d), and 3–12 (e, f) on the northwestern, northern, and northeastern sides of Hanna Shoal, respectively. Fig. 1 shows transect locations. Hanna Shoal is on the left of each panel.

section.

Several features are common to all sections. First, below ~ 20 m depth the water column consists entirely of WW with salinities > 32.5 and temperatures < − 1.6 °C. In 2012, salinities within 10–15 m of the bottom exceeded 33, with maximum salinities (> 33.4) near the bottom on Section 1–12 (Fig. 9b). Bottom salinities rarely exceeded 33 in 2013. Second, in general the surface layer consisted of meltwater with low salinities (< 30) and temperatures between − 0.5 °C and 0.5 °C. Third, along the northern side of the Shoal and proceeding from west to east, the salinities in the upper 10 m decreased by ~ 2. Fourth, the 2-layer stratification of the water column was set by a strong halocline centered between 10 and 15 m depth.

There are a number of exceptions to these general features. First, warmer (1–2 °C), near surface waters were observed south of Hanna Shoal at the southern end of Sections 4–12, 5–12, and 4–13 (Fig. 11). Each of these sections extended as far south as ~ 71.5°N, suggesting that the warm water source was BSSW intruding across the front (Fig. 4).

Second, warm (> 0 °C) surface or near surface waters were found within the first 35 km of sections 1–12 (Figs. 9a) and 1–13 (Fig. 10a) along stations nearest to the Shoal. In both cases, the warmest water was in a subsurface temperature maximum embedded in the pycnocline. These warm waters were likely BSSW, albeit modified by meltwaters, which had flowed northward through the Central Channel and had begun to flow clockwise around the northern side of the Shoal. This interpretation is consistent with velocities at moorings HSNW-40 and -50 in 2012 where the mean flow was ~ 7 cm s^{-1} toward the east-northeast during the time that Sections 1–12 to 3–12 were occupied. In 2013, this flow averaged ~ 5 cm s^{-1} eastward over the time required to occupy Sections 1–13 to 3–13. (In both years the flow was largely barotropic insofar as the velocity shears were small; the differences between the near-surface and near-bottom ADCP bins were ~ 3 cm s^{-1}.) However, subsurface temperature maxima were absent along the sections further east. In 2012 the warmest waters along 2–12

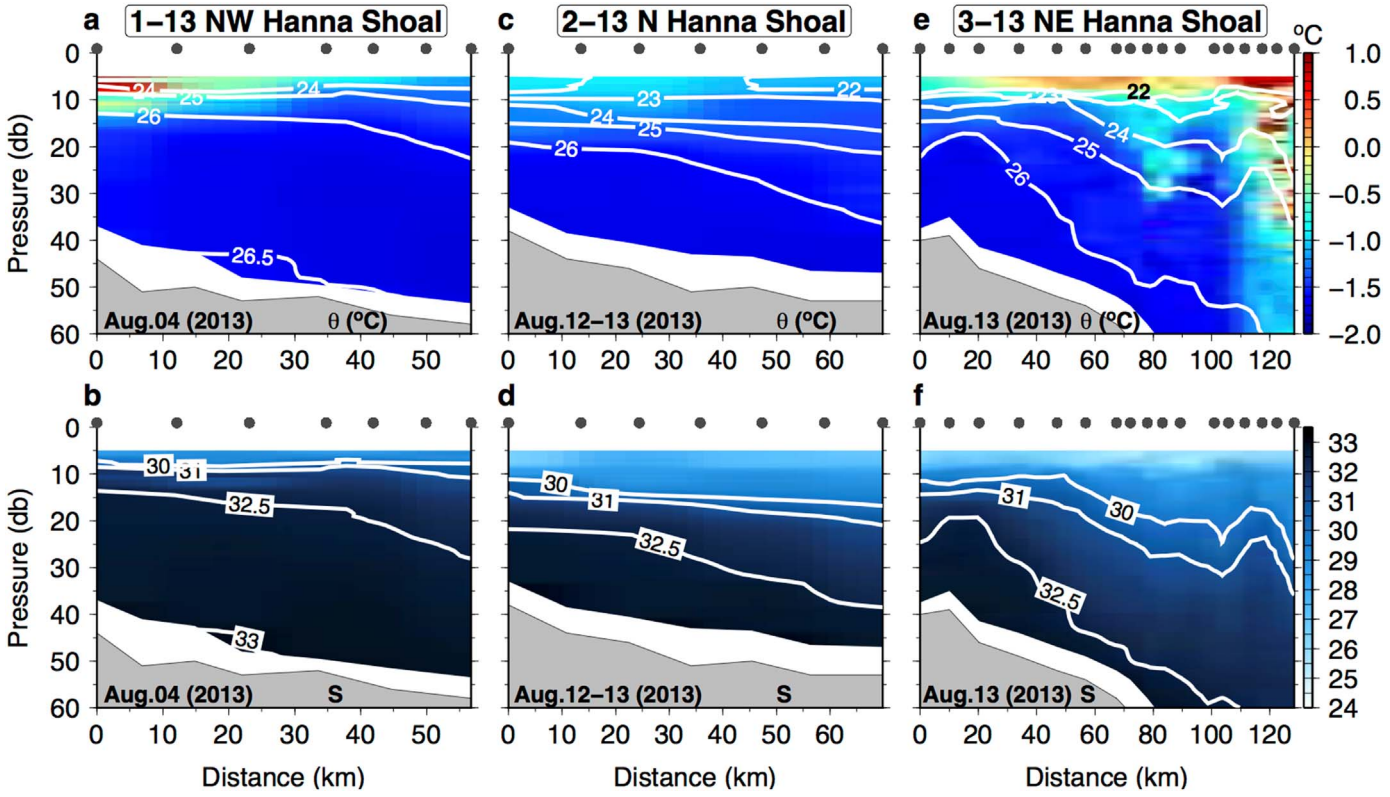

Fig. 10. As in Fig. 9 but for transects 1–13 (a, b), 2–13 (c, d), and 3–13 (e, f) on the northwestern, northern, and northeastern sides of Hanna Shoal, respectively. Fig. 1 shows transect locations. Hanna Shoal is on the left of each panel.

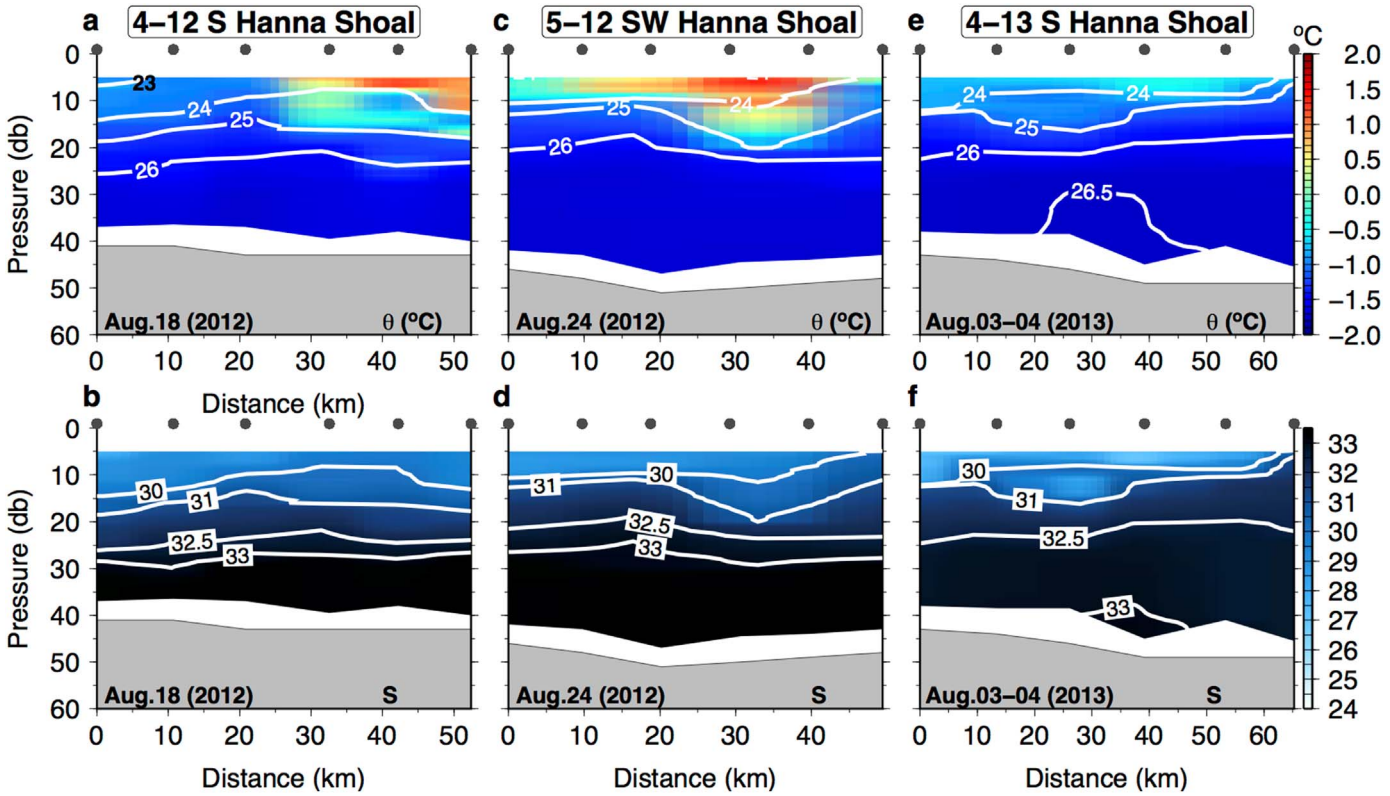

Fig. 11. As in Fig. 9 but for transects 4–12 (a, b), 5–12 (c, d), and 4–13 (e, f). Panels a, b, e, and f are on the southern side of Hanna Shoal, and panels c and d are on the southeastern side. Fig. 1 shows transect locations. Hanna Shoal is on the left of each panel. Note the temperature scale differs from that of Figs. 9 and 10.

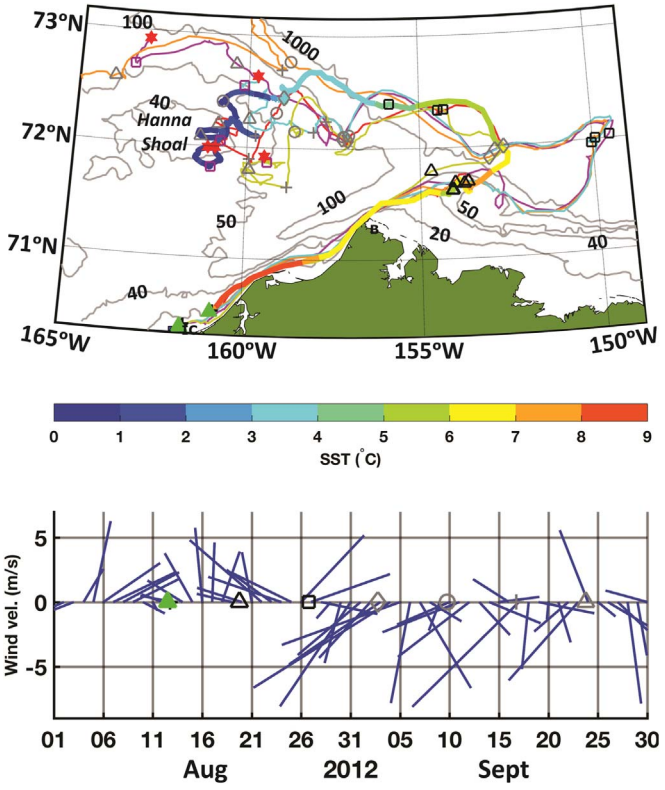

Fig. 12. The trajectories of 6 satellite-tracked drifters (1-m drogue depth) deployed offshore of Icy Cape on 12 August 2012. One of the trajectories is color-coded according to measured SST. The various symbols along each trajectory are at 7-day intervals with the dates given on the wind vector time series (bottom plot). The 20, 40, 50, 100 and 1000 m isobaths are labelled. Green triangles signify the deployment position and red stars the last good transmission from each drifter. (For interpretation of the references to color in this figure legend, the reader is referred to the web version of this article.)

(Fig. 9c) were at the distal end of the section, whereas on 2–13 the warmest water was adjacent to the Shoal. We argue later that these warm signals are likely a mixture of the waters from the western and northeastern sides of the Shoal.

Third, surface waters over the outer parts of sections 3–12 and 3–13 were also warm and fresh, suggesting that these were either meltwaters that had warmed by solar radiation or were derived from the Alaska Coastal Current emanating from Barrow Canyon. Corlett and Pickart (2017) reported the presence of coastal waters flowing westward in the Chukchi Slope Current. Here we show that the coastal waters can, at least occasionally, be transported from the Chukchi Slope Current onto the shelf northeast of Hanna Shoal and thence continue westward on the shelf and/or southward over the Shoal. Fig. 12 shows the sea surface temperature (SST) color-coded trajectories for 6 of the 13 total drifters between 12 August 2012 (when they were deployed in the Alaskan Coastal Current near Icy Cape) and 30 September, along with the winds for the same time period. Upon deployment, the winds were southerly and the drifters moved rapidly through Barrow Canyon. At the mouth of the canyon, all but one eventually moved westward in the slope current. Six of the drifters (those shown in Fig. 12) crossed back onto the shelf northeast of Hanna Shoal after the winds became northeasterly on ~ 31 August, while the remaining six continued westward along the slope. SSTs decreased from ~ 10 °C at deployment to 2–3 °C by mid-September on the shelf north and east of Hanna Shoal. For those drifters that continued farther south, the SST decreased to ~ < 0 °C by month's end. The cooling was most likely due to mixing between the coastal water and MW along the drifter path and, beginning mid-September, due to heat loss to the atmosphere.

The final noteworthy difference among the COMIDA CTD sections is that the slopes of the subsurface isopycnals differ around the Shoal. On the south side of the Shoal the isopycnal slopes were nearly flat indicating very little baroclinicity. On the north side and below the pycnocline, the isopycnals on sections 1–12, 3–12, 1–13, 2–13, and 3–13 slope downward away from the Shoal. The largest slopes were below the pycnocline along sections 3–12 and 3–13, both on the northeast side of Hanna Shoal. As shown below these slopes imply a baroclinic velocity field that likely plays an important role in the circulation north of Hanna Shoal.

3.4. The north side of Hanna Shoal

In this section we seek to understand the source of the warm surface waters on the north side of the Shoal, specifically along sections 2–12 and 2–13. Recall that these waters are cooler than those on either the northwest or northeast sides of the Shoal. We first consider the possibility that these waters simply resulted from the cooling of warm waters from the Central Channel flowing around the northwest side of the Shoal across sections 1–12 and 1–13. We examine this possibility by computing the horizontal heat flux divergence of the warm water band over the upper 15 m and over a horizontal width of 30 km (essentially the width of the warm water flowing from the Central Channel) and assume only vertical heat exchanges occur, to either the ice or to the water column below 15 m. The calculation uses the velocity averages given previously and also assumes the warm water at the outer end of Section 2–12 entirely captured the remnants of the warm waters flowing through Section 1–12. In 2012, the heat flux calculations imply a heat loss to the ice of ~ 20 W m^{-2}, for an ice melt rate of 0.6 cm day^{-1}. The advective time scale between sections 1–12 and 2–12 is ~ 10 days, which would result in the addition of 6 cm of meltwater to the upper 15 m. Assuming a sea ice salinity of 5; this meltwater flux would reduce the salinity by 0.1 between the two sections, which is far less than the observed salinity decrease of ~ 0.8. Moreover, the additional ice melt influx required to satisfy the salinity change implies an atmospheric heating rate of ~ 185 W m^{-2}. For a surface ice albedo of 0.6, the required solar radiative influx amounts to ~ 300 W m^{-2}. These values seem unrealistically high even in the absence of the dense fog present in the area at the time. For example, on a monthly basis, Maykut (1986) estimates that the net radiation balance in mid-summer is ~ 100 W m^{-2}. The same calculation for the 2013 data yields a similar conclusion, e.g., the solar radiative influx is much greater than feasible. We conclude the salinity imbalance implies an advective contribution of meltwater from elsewhere, most likely from the northeast side of the Shoal.

There are two lines of evidence to support this contention. The first follows from the θ/S diagrams compiled from Sections 1, 2 and 3 from each year (Fig. 13) over the upper 30 m of the water column. Included in this figure are the average θ/S values in the upper 15 m encompassing the warm waters along each section. Clearly the surface water properties along Section 2–12 could be obtained by cooling and mixing of the surface waters from the eastern and western sides of the Shoal. In 2013, the warm band along Section 2–13 was ~ 0.3 °C cooler than that on the northeast side of the Shoal, and the salinities were identical at ~ 28.7. In contrast the salinity on the northwest side of the Shoal was, at ~ 30.8, much greater.

The second line of evidence follows from the baroclinic geostrophic tendencies along sections 3–12, 2–13, and 3–13 (Fig. 14). (Baroclinicity along Section 2–12 is weak and variable and, thus, not shown). In 2012, the baroclinic tendency was northwestward along Section 3–12, and, over the outer half of the section, averaged ~ 5 cm s^{-1} in the upper 20 m. Along the 40 m isobath, the tendency was southeastward at ~ 5 cm s^{-1}. These values are in good agreement with currents measured by the moorings deployed during occupation of the section. During the first three days after deployment, the currents in the upper 20 m were west-northwest currents at 6 and 13 cm s^{-1} over the 50 and 56 m isobaths, respectively. There was similar agreement between the computed and measured velocity shears as well. The velocity difference

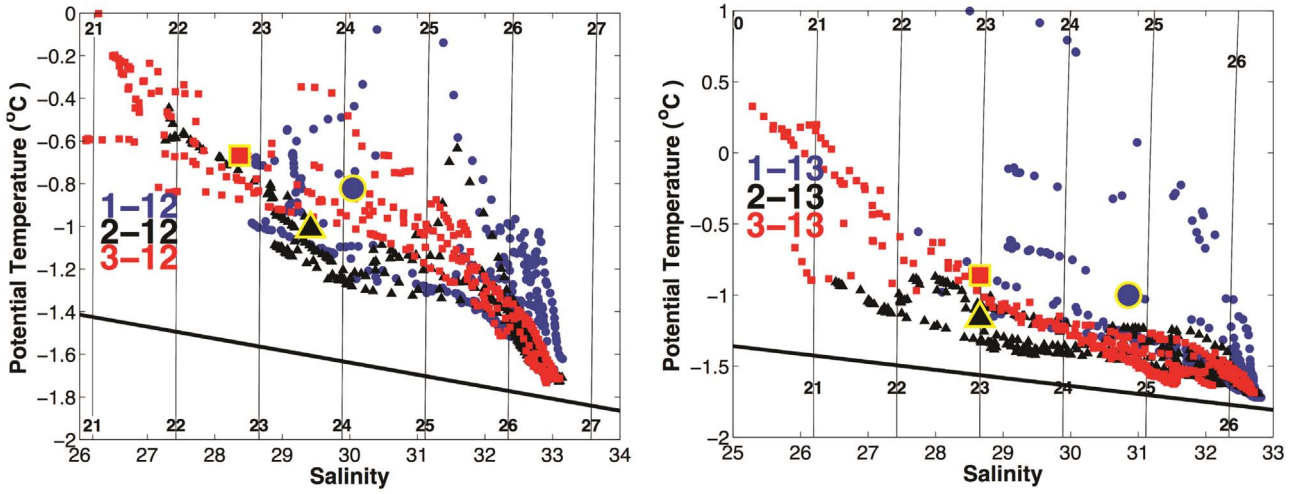

Fig. 13. Scatterplots of potential temperature versus salinity over the upper 30 m of the water column for Sections 1, 2, and 3 in 2012 (left) and 2013 (right). Only stations along the first 65 km of the transect are included. Note the scales change between 2012 and 2013. The black slanted line denotes the freezing point curve. The larger symbols outlined in yellow depict the mean values along each section in the upper 15 m. (For interpretation of the references to color in this figure legend, the reader is referred to the web version of this article.)

over the 25 m between 20 and 45 m depth at the two moorings were ~ 10 cm s^{-1} compared to ~ 6 cm s^{-1} based on the thermal wind estimates. The mooring deployed on the 40 m isobath recorded 3 cm s^{-1} toward the west-southwest.

In 2013, the geostrophic computations yielded results similar to those of 2012 between the 40 and 60 m isobaths. The calculations also indicate that the baroclinic tendency increased to ~ 10 cm s^{-1} over the deeper part of the section. The moored measurements averaged over the upper 25 m of the water column during the transit of this section in 2013 section were ~ 5 cm s^{-1} to the southwest over the 40 m isobath and ~ 10 cm s^{-1} northwestward on the 50 m isobath (the ADCP moored on the 56 m isobath died a month earlier). The baroclinic contribution was weaker along Section 2–13 (north of Hanna Shoal) although still westward. In summary our results suggest that there was zonal convergence, at least along the 50 m isobath and over the upper portion of the water column, north of Hanna Shoal in August of both 2012 and 2013.

4. Discussion

Our analyses clearly highlight the importance of sea ice, meltwaters, and dense water to the hydrographic structure of the northeastern Chukchi Sea, particularly in the Hanna Shoal region. Meltwater was absent in 2011, consistent with early ice retreat and the absence of ice over the Shoal in August. The heavy and persistent ice concentrations over Hanna Shoal in 2012 and 2013 resulted in a ~ 15 m thick cap of dilute meltwater sitting above much denser winter water over most of the shelf north of ~ 71.5°N. As a consequence the shelf stratification was substantially greater in 2012 and 2013 than in 2011. A front extending from the southwest side of Hanna Shoal (along ~ 71.5°N) eastward to Barrow Canyon separated the meltwater region from BSSW to the south. The meltwater pool north of the front supported substantially more mesoscale and sub-mesoscale surface layer density variations than the waters south of the front. In the absence of meltwater in 2011, we presume that surface density variability was comparatively small during that summer.

We suggest that the enhanced variability in the meltwater region in 2012 and 2013 may be a result of two distinct causes. The first is due to instability of the MW/BSSW front (Lu et al., 2015), which is expected to enhance the variance at the longer length scales and subsequently, through forward cascade (McWilliams, 2008), to smaller length scales. The second may arise as a consequence of the ice floe size distribution, which changes seasonally. Winter floes tend to be large and consolidated, whereas in summer, floe consolidation decreases, and floe

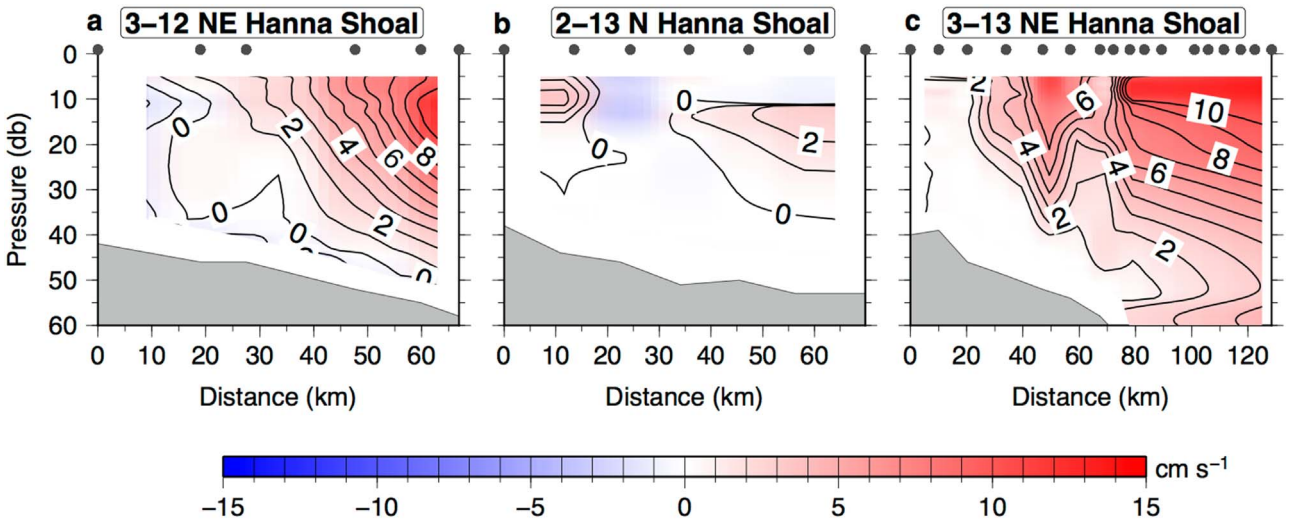

Fig. 14. Baroclinic, geostrophic velocity field for transects a) 3–12, b) 2–13, and c) 3–13. The corresponding temperature and salinity sections are shown in Figs. 9e, f; 10b, d; and 10 e, f, respectively. Positive velocities are north-northwestward and negative values are south-southeastward.

areas and thicknesses span a broader range (Perovich and Jones, 2014). Spatial heterogeneity in the ice thickness distribution implies variations on similar spatial scales in the ice-ocean drag and melt rates. In August of 2012 and 2013, Hanna Shoal was covered by consolidated and grounded ice spanning 10 s of km^2, as well as regions containing smaller, unconsolidated floes interspersed with leads. The buoyant meltwater plumes formed should vary in size accordingly, thus contribute to the surface density variance wavenumber spectrum. Different plume sizes are subject to different dynamical constraints; those within the mesoscale range are subject to rotation while ageostrophic dynamics are important over the sub-mesoscale portion of the spectrum (Yankovsky and Yashayaev, 2014).

What caused the differences in Hanna Shoal summer ice conditions across the 2011 – 2013 period? While we cannot provide a definitive answer, we offer several possibilities. First we note that the northward heat transport through Bering Strait was substantially greater in 2011 than in 2012 and 2013 (Woodgate et al., 2012, 2015), which suggests that the ocean heat flux to the ice was greater in 2011. Indeed, the 2011 heat flux through Bering Strait was as large as that in 2007, when ice retreat across the Chukchi Sea shelf was also unusually early (Woodgate et al., 2010). Persistent northeasterly winds observed in summer 2011 favors the westward drift of ice (Spall, 2007). These winds would also force a westward drift (Pisareva et al., 2015) of newly exposed surface waters heated by solar radiation and an ever-increasing fetch over which waves would be generated. Both factors would enhance ice-edge retreat. We have also examined solar radiation differences amongst these summers and find that this variable alone cannot account for the differences among years. For example, NARR incoming solar radiation estimates from Bering Strait and the southern and northeastern Chukchi shelf indicate that the mean daily June and July values in 2012 exceeded that of the other years by ~ 40 W m^{-2}, and yet ice concentrations were quite high that summer.

While northeasterly winds in the early part of summer 2011 may have played a role in ice retreat, the heavy ice concentrations over Hanna Shoal in 2012 and 2013 do not appear to be related to the August winds. In August 2012, mean winds were southerly at 1 m s^{-1}, whereas in 2013, the mean August winds were northeasterly at 2 m s^{-1} (Fig. 2c–f). Additionally ice conditions on Hanna Shoal do not correspond to ice concentrations in the Arctic basin. According to the NIC, the heavy ice concentrations in summer 2012 occurred when the arctic-wide sea ice extent was the third lowest over the 1979–2013 period, with only the summers of 2007 and 2011 having lower ice concentrations. Indeed, in 2012, the entire Beaufort Sea shelf and slope were ice-free while Hanna Shoal was covered by thick ice at high concentrations.

Another factor affecting Hanna Shoal summer ice conditions may be processes that occurred the previous winter. In both August 2012 and 2013 thick ice was grounded atop Hanna Shoal. According to A. Mahoney [pers. comm.], grounding was evident over Hanna Shoal in late winter of both years. Eicken and Mahoney (2015) maintain that the source of this grounded ice is westward-drifting, heavily deformed ice from the eastern Beaufort and/or from a heavily-ridged ice arch that often protrudes north of Pt. Barrow. Ice keels must be ~ 20 m in order to ground on the shallower portions of the Shoal. Sufficiently thick and deformed ice does not typically occur in the Beaufort Sea until January, at the earliest [H. Eicken, per. comm.]. Once firmly grounded ice is established over Hanna Shoal, additional ice, even if thin, may collide and adhere on the windward side of the grounding zone. In this scenario the initial grounding subsequently promotes consolidation and additional ice deformation, which leads to heavy concentrations of thick ice that persist through summer.

There is indirect support for this hypothesis based on the mean January through April winds and ice drift derived from moored ADCP and IPS data (Fig. 15). Fig. 15b, d, and f show the mean winds and sea level pressure over the northern Bering and Chukchi Seas from January through April of 2011, 2012, and 2013. In 2011, the mean winds were weak (< 1 m s^{-1}) and southerly. In contrast, the mean winds in 2012 were north-northeasterly at 2–3 m s^{-1}, and in 2013 they were northeasterly at 3–5 m s^{-1}. These differences are reflected in the mean monthly ice velocity and variance ellipses for January through April of each year (Fig. 15a, c, and e). In the winter of 2011, the ice drift was northeastward in accordance with mean currents in these areas (Weingartner et al., 2005). Although the drift east and north of Hanna Shoal may have been different, the mean winds were clearly unfavorable for ice advection from the Beaufort Sea. In contrast the ice drift in the winter of 2012 was southwesterly at ~ 5 cm s^{-1} at all sites and in 2013 the drift was westerly at ~ 5–10 cm s^{-1}. Although the interannual differences in drifts corroborate this hypothesis, the results based on the mean keel depths using only the upper 25% of the ice keel distributions are less supportive. In each year the largest of these means occurred in March and April and there was generally little spatial variability amongst sites. In 2011 and 2013 the values were 14.5 m and in 2012 they were 21 m. On this basis, it appears that 2012 was more favorable for ice grounding on the Shoal than in the other years.

Our measurements indicate that in all three years the densest winter water surrounded the Shoal. The source of this dense water is somewhat uncertain, however. One conceivable source is local formation over the Shoal during the preceding winter, as polynyas can form in the lee of grounded ice (Mahoney et al., 2012). Alternatively, brine repulsion from leads over the shallow Shoal would enhance local dense water formation. Under either circumstance, the dense water would be trapped to the Shoal and, in the absence of additional forcing, circulate anticyclonically around the Shoal (Spall, 2013). However, the summer synoptic shipboard measurements of Pickart et al. (2016) and the annually averaged measurements from moorings in 2011 (Weingartner et al., 2017) along the south side of the Shoal suggest a mean flow of ~ 2 cm s^{-1} to the southeast, which would transport the dense water toward Barrow Canyon. On the northwest side of the Shoal, the mean annual flow is northeastward at ~ 5 cm s^{-1} (unpublished data). Although the vertically-averaged flow on the northeast side of the Shoal is not significantly different from zero (Weingartner et al., 2017), the mean bottom flow is southward at ~ 2 cm s^{-1} (unpublished data) The smaller of these values implies an advective time scale of 75 days for the movement of bottom waters from the west to the east side of the Shoal. If all of this dense water resulted solely from local ice formation processes, this time scale implies that the dense water surrounding the Shoal should have been absent by August assuming freezing ends in mid-May as suggested by climatology (Maykut, 1986). The presence of dense water well into September suggests another advective source that transports dense waters toward the Shoal from either the Central Channel and/or Herald Valley (Pickart et al., 2010). Regardless of the source, there were considerable interannual differences in dense water salinities with the saltiest (~ 33) water observed in 2012 and the least salty (~ 32.5) in 2011. These differences may affect the vertical stratification in the following summer and perhaps the strength of the baroclinic flow on the northeast side of the Shoal.

5. Conclusion

Hydrographic data from the northeastern Chukchi shelf collected in August and September of 2011–2013 showed large interannual variations in the hydrographic properties surrounding Hanna Shoal. These differences primarily relate to the salinities of the bottom waters and to the presence or absence of surface meltwaters. The latter is tied to processes that govern summer ice retreat and, as hypothesized here, to the previous winter's history of ice advection, which may control grounding on the Shoal. We also found a northwestward baroclinic flow on the northeast side of the Shoal, which opposed the model-predicted clockwise barotropic motion around the northwest side of the Shoal. These opposing flow tendencies suggest zonal flow convergence on the north side of the Shoal, which implies that the vertically-integrated meridional pressure gradient must vanish or otherwise adjust to these opposing tendencies. If convergence is a persistent feature of the

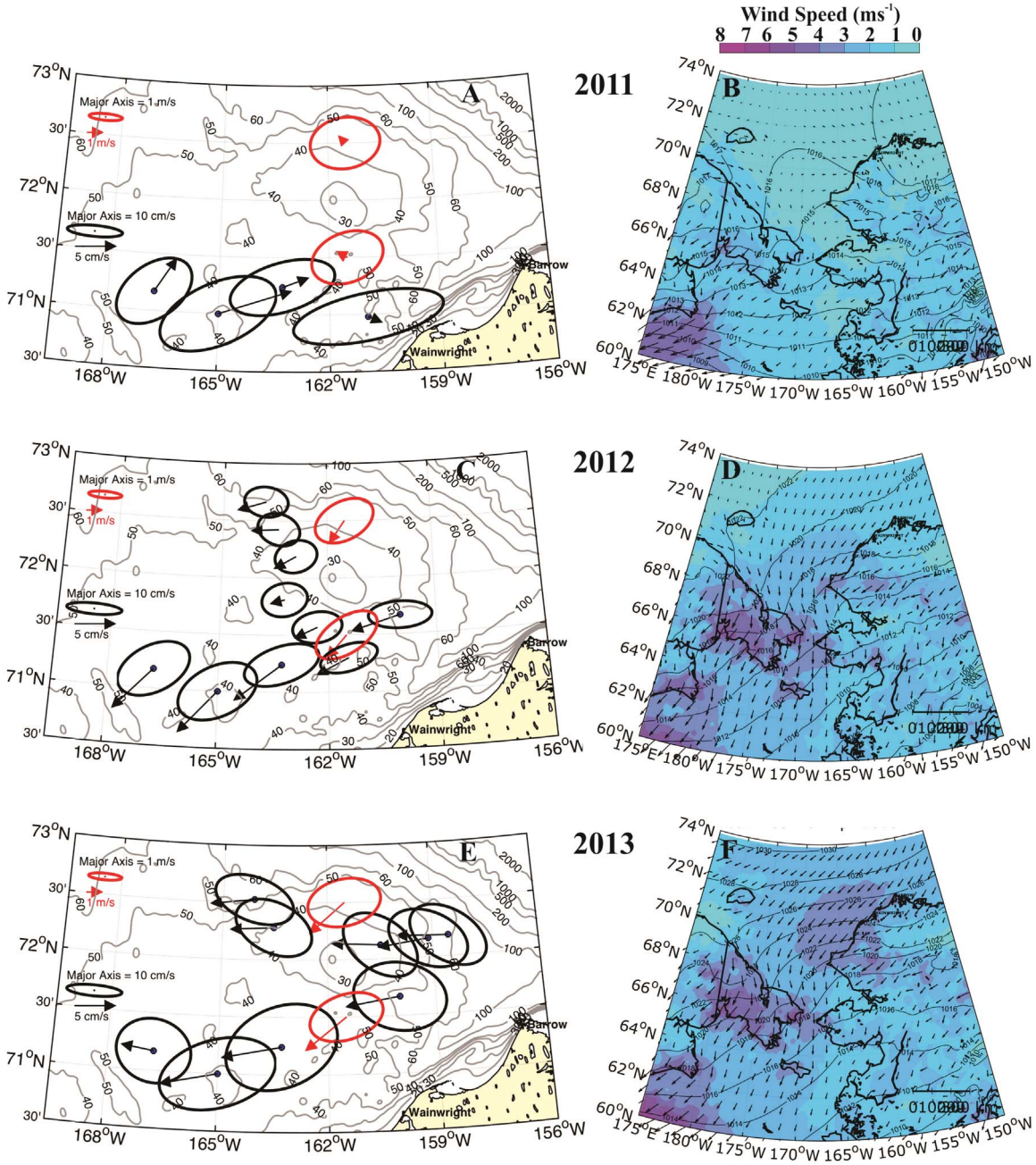

Fig. 15. Each row shows the mean January – March ice and wind velocities (left panels) and regional wind vectors and sea level pressure (right side) over the northern Bering and Chukchi seas for 2011 (top row), 2012 (middle row), and 2013 (bottom row). Black arrows and ellipses denote the mean ice velocity and the corresponding velocity variance ellipses, while the red arrows and ellipses are for the winds.

circulation here then the region north of Hanna Shoal may be a site of enhanced cross-shelf transport.

Acknowledgements

This work was supported by the Bureau of Ocean Energy Management (BOEM) Cooperative Agreements M11AC00007 and M12AC00008. Under the aegis of the Chukchi Sea Environmental Studies Program (CSESP), ConocoPhillips Alaska Inc., Shell Exploration and Production, Inc., and Statoil USA Exploration and Production supported the broad-scale hydrography, the ADCP-IPS moorings south and east of Hanna Shoal, and all the moorings in 2011. The North Slope Borough-Shell Baseline Studies Program supported the drifter program. Billy Adams, Willard Neatok, and Robert Suydam assisted in the drifter deployments and Cayman Irving helped process these data. Shenya Wisdom and Olgoonik Fairweather Inc. efficiently coordinated the CSESP field programs. We thank the officers and crews of the USCGC *Healy*, *Westward Wind*, and *Norseman II* for ensuring safe operations at sea. The NARR data was obtained from the NOAA/OAR/ESRL PSD, Boulder, Colorado, USA, (http://www.esrl.noaa.gov/psd/). We thank the Sea Ice Remote Sensing group at the University of Bremen and the U.S. National Ice Center for providing access to the sea ice data sets.

References

Bockstoce, J.R., 1986. Whales, Men, and Ice: The History of Whaling in the Western Arctic. University of Washington Press, Seattle, WA.

Blanchard, A.L., Parris, C.L., Knowlton, A.L., Wade, N.R., 2013. Benthic ecology of the northeastern Chukchi Sea. Part II. Spatial variation of megafaunal community

structure, 2009–2010. Cont. Shelf Res. 2009–2010.
Coachman, L.K., Aagaard, K., Tripp, R.B., 1975. Bering Strait: The Regional Physical Oceanography. Univ. of Washington Press, Seattle, pp. 172.
Codispoti, L., Flagg, C., Kully, V., Swift, J.H., 2005. Hydrographic conditions during the 2002 SBI process experiments. Deep-Sea Res. II 52 (24–26), 3199–3226.
Corlett, W.B., Pickart, R.S., 2017. The Chukchi slope current. Prog. Oceanogr. 153, 50–65. http://dx.doi.org/10.1016/j.pocean.2017.04.005.
Danielson, S.L., Eisner, L., Ladd, C., Mordy, C., Sousa, L., Weingartner, T.J., 2017. A comparison between late summer 2012 and 2013 water masses, macronutrients, and phytoplankton standing crops in the northern Bering and Chukchi Seas. Deep-Sea Res. II 135, 7–26.
Davis, R.E., 1985. Drifter observations of coastal surface currents during CODE: the method and descriptive view. J. Geophys. Res. 90, 4741–4755.
Eicken, H., Mahoney, A.R., 2015. Sea ice: hazards, risks, and implications for disasters. In: Ellis, J.T., Sherman, D.J. (Eds.), Sea and Ocean Hazards, Risks, and Disasters. Elsevier, Oxford, United Kingdom, pp. 381–401. http://dx.doi.org/10.1016/B978-0-12-396483-0.00013-3.
Fang, Y.-C., Potter, R.A., Statscewich, H., Weingartner, T.J., Winsor, P., Irving, B.K., 2017. Surface current patterns in the northeastern Chukchi Sea and their response to wind forcing. J. Geophys. Res.
Grantz, A., Eittreim, S., 1979. Geology and Physiography of the Continental Margin North of Alaska and Implications for the Origin of the Canada Basin U.S. Geological Survey, Open-File Report 79-288. pp. 61.
Gong, D., Pickart, R.S., 2014. Summertime circulation in the eastern Chukchi Sea. Deep Sea Res. II 118, 18–31.
Lu, K., Weingartner, T., Danielson, S., Winsor, P., Dobbins, E., Martini, K., Statscewich, H., 2015. Lateral mixing across ice meltwater fronts of the Chukchi Sea shelf. Geophys. Res. Lett. 42, 6754–6761. http://dx.doi.org/10.1002/2015GL064967.
Mahoney, A.R., Eicken, H., Shapiro, L.H., Gens, R., Heinrichs, T., Meyer, F., Graves, J., Gaylord, A., 2012. Mapping and Characterization of Recurring Spring Leads and Landfast Ice in the Beaufort and Chukchi Seas. OCS Study BOEM 2012-067. U.S. Dept. of the Interior, Bureau of Ocean Energy Management, Alaska Region, Anchorage, AK, pp. 179.
Martin, S., Drucker, R., 1997. The effect of possible Taylor columns on the summer sea ice in the Chukchi Sea. J. Geophys. Res. 102 (5), 10473–10482.
Martini, K.I., Stabeno, P.J., Ladd, C., Winsor, P., Weingartner, T.J., Mordy, C.W., Eisner, L.B., 2016. Dependence of subsurface chlorophyll on seasonal water masses in the Chukchi Sea. J. Geophys. Res. Ocean 121 (3), 1755–1770. http://dx.doi.org/10.1002/2015JC011359.
Maykut, G.A., 1986. The surface mass and heat balance. In: Unstersteiner, N. (Ed.), The Geophyics of Sea Ice. Plenum Press, New York, pp. 395–463.
McWilliams, J.C., 2008. Fluid dynamics at the margin of rotational control. Environ. Fluid Mech. 8, 441–449.
Melling, H., Johnston, P.H., Riedel, D.A., 1995. Measurement of the draft and topography of sea ice by moored subsea sonar. J. Atmos. Ocean. Technol. 13, 589–602.
Mesinger, F., et al., 2006. North American regional re-analysis. Bull. Am. Meteorol. Soc. 87, 343–360.
Moore, S.E., Huntington, H.P., 2008. Arctic marine mammals and climate change: impacts and resilience. Ecol. Appl. 18 (Suppl. 2), 157–165.
Moore, S.E., Stabeno, P.J., Grebmeier, J.M., Okkonen, S.R., 2017. The Arctic Marine Pulses Model: linking annual oceanographic processes to contiguous ecological domains in the Pacific Arctic. Deep Sea Res. II. http://dx.doi.org/10.1016/j.dsr2.2016.10.011. (in press).
Mudge, T.D., Fissel, D.B., Sadowy, D., Borg, K., Billenness, D., Knox, K., Slonimer, A., Batistuzzo, H., Milutinovic, N., Clouston, R., Martinez, M., Barrette, J., Kulan, N., 2015. Analysis of Ice and Metocean Measurements, Chukchi Sea 2013–2014, for Shell. Project Report for Shell International Exploration and Production Inc., Houston, Texas by ASL Environmental Sciences Inc., Victoria, B.C. Canada. xi +, p. 108.
Paquette, R.G., Bourke, R.H., 1981. Ocean circulation and fronts as related to ice melt-back in the Chukchi Sea. J. Geophys. Res. 86, 4215–4230.
Perovich, D.K., Jones, K.F., 2014. The seasonal evolution of sea ice floe size distribution. J. Geophys. Res. 119, 8767–8777. http://dx.doi.org/10.1002/ 2014JC010136.
Pickart, R.S., Weingartner, T.J., Pratt, L.J., Zimmermann, S., Torres, D.J., 2005. Flow of winter-transformed Pacific water into the Western Arctic. Deep-Sea Res. II 52 (24–26), 3175–3198. http://dx.doi.org/10.1016/j.dsr2.2005.10.009.
Pickart, R.S., Pratt, L.J., Torres, D.J., Whitledge, T.E., Proshutinsky, A.Y., Aagaard, K., Agnew, T.A., Moore, G.W.K., Dail, H.J., 2010. Evolution and dynamics of the flow through Herald Canyon in the Western Chukchi Sea. Deep-Sea Res. II 57, 5–26.
Pickart, R.S., Moore, G.W.K., Mao, C., Bahr, F., Nobre, C., Weingartner, T.J., 2016. Circulation of winter water on the Chukchi shelf in early summer. Deep-Sea Res. II 130, 56–75. http://dx.doi.org/10.1016/j.dsr2.2016.05.001.
Pisareva, M.N., Pickart, R.S., Spall, M.A., Nobre, C., Torres, D.J., Moore, G.W.K., Whitledge, T.E., 2015. Flow of Pacific water in the western Chukchi Sea: results from the 2009 RUSALCA expedition. Deep-Sea Res. I 105, 53–73. http://dx.doi.org/10.1016/j.dsr.2015.08.011.
Questel, J.M., Clarke, C., Hopcroft, R.R., 2013. Seasonal and interannual variation in the planktonic communities of the northeastern Chukchi Sea during the summer and early fall. Cont. Shelf Res. 67, 23–41.
Schonberg, S.V, Clarke, J.T., Dunton, K.H., 2014. Distribution, abundance, biomass and diversity of benthic infauna in the northeast Chukchi Sea, Alaska: relation to environmental variables and marine mammals. Deep-Sea Rese. II 102, 144–163. http://dx.doi.org/10.1016/j.dsr2.2013.11.004 2014.
Spall, M.A., 2013. Dense water formation around islands. J. Geophys. Res. Oceans 118, 2507–2519. http://dx.doi.org/10.1002/jgrc.20185.
Spall, M.A., 2007. Circulation and water mass transformation in a model of the Chukchi Sea. J. Geophys. Res. 112, C05025. http://dx.doi.org/10.1029/2005JC002264.
Spreen, G., Kaleschke, L., Heygster, G., 2008. Sea ice remote sensing using AMSR-E 89 GHz channels. J. Geophys. Res. 113, C02S03. http://dx.doi.org/10.1029/2005JC003384.
Thomas, L.N., Taylor, J.R., Ferrari, R., Joyce, T.M., 2016. Symmetric instability in the Gulf stream. Deep-Sea Res. II 91, 96–110.
Timmermans, M.-L., Winsor, P., 2012. Scale of horizontal density structure in the Chukchi Sea surface layer. Cont. Shelf Res. 52, 39–45.
Weingartner, T.J., Potter, R.A., Stoudt, C.A., Dobbins, E.L., Statscewich, H., Winsor, P.R., Mudge, T.D., Borg, K., 2017. Transport and thermohaline variability in Barrow Canyon on the northeastern Chukchi Sea shelf. J. Geophys. Res. http://dx.doi.org/10.1002/2016JC012636.
Weingartner, T., Irvine, C., Dobbins, E.L., Danielson, S., Sousa, L., Adams, B., Suydam, R., Neatok, W., 2015. Satellite-Tracked Drifter Measurements in the Chukchi and Beaufort seas. Final Report, OCS Study 2015–022. Bureau of Ocean Energy Management, Anchorage, Ak, USA, pp. 171. 〈http://www.boem.gov/Alaska-Reports-2015/〉.
Weingartner, T., Danielson, S., Dobbins, E., 2014. Physical Oceanographic Measurements in the Northeastern Chukchi Sea: 2013. Technical Report Prepared for ConocoPhillips, Inc. Shell Exploration & Production Company and Statoil USA E & P, Inc., pp. 52.
Weingartner, T., Dobbins, E., Danielson, S., Potter, R., Statscewich, H., Winsor, P., 2013. Hydrographic variability over the northeastern Chukchi Sea shelf in summer-fall 2008–2010 (http://dx.doi.org/). Cont. Shelf Res. http://dx.doi.org/10.1016/j.csr.2013.03.012.
Weingartner, T., Aagaard, K., Woodgate, K., Danielson, R., Sasaki, S., Cavalieri, D, Y., 2005. Circulation on the north central Chukchi Sea shelf. Deep-Sea Res. Part II 52 (24–26), 3150–3174.
Winsor, P., Chapman, D.C., 2004. Pathways of Pacific Water across the Chukchi Sea: a numerical model study. J. Geophys. Res. 109, C03002(doi: http://dx.doi.org/1029/2003JC001962).
Woodgate, R.A., Stafford, K.M., Prahl, F.G., 2015. A Synthesis of year-round interdisciplinary mooring measurements in the Bering Strait (1990–2014) and the RUSALCA years (2004–2011). Oceanography 28 (3), 46–67. http://dx.doi.org/10.5670/oceanog.2015.57.
Woodgate, R.A., Weingartner, T.J., Lindsay, R., 2012. Observed increases in Bering Strait oceanic fluxes from the Pacific to the Arctic from 2001 to 2011 and their impacts on the Arctic Ocean water column. Geophys. Res. Lett. 39 (24), 6. http://dx.doi.org/10.1029/2012gl054092.
Woodgate, R.A., Weingartner, T., Lindsay, R., 2010. The 2007 Bering Strait oceanic heat flux and anomalous Arctic sea-ice retreat. Geophys. Res. Lett. 37. http://dx.doi.org/10.1029/2009GL041621.
Woodgate, R.A., Aagaard, K., Weingartner, T., 2005. A year in the physical oceanography of the Chukchi Sea: Moored measurements from autumn 1990-91. Deep-Sea Res. Part II 52 (24–26), 3116–3149.
Yankovsky, A.E., Yashayaev, I., 2014. Surface buoyant plumes from melting icebergs in the Labrador Sea. Deep-Sea Res. I 91, 1–9.